Tanzania Journal of Science 50(5): 1099-1119, 2024
ISSN 0856-1761, e-ISSN 2507-7961

Analysis of Unsteady Convective Boundary Layer Flow with Magnetic fields, Chemical reaction, Thermal Radiation and Variable fluid Properties

Jonas A. James[1, 2*], Makungu J. Ng'oga[2], Augustino I. Msigwa [2], Ali A. Omary [3]
[1]*Institute of Accountancy Arusha, Department of Informatics, Tanzania*
[2]*University of Dar es Salaam, Department of Mathematics, Tanzania*
[3]*Ardhi University, Department of Mathematics, Tanzania*
Emails: jonasjames635@gmail.com, makungujbuza@gmail.com, lukwea@yahoo.com, ahmada.omar54@gmail.com.
**Corresponding author: (jonasjames635@gmail.com.*
Received 25 Aug 2024, Revised 7 Nov 2024, Accepted 17 Dec 2024, Published 31 2024
https://dx.doi.org/10.4314/tjs.v50i5.15

Abstract

This study extends the previous work by Kitengeso et al. (2018) by investigating unsteady convective boundary layer flow, incorporating magnetic fields, chemical reactions, radiation, and variable fluid properties over the inclined plate. The boundary layer and Boussinesq approximations are used to derive the magnetohydrodynamic flow equations. Thereafter, the equations are transformed into similarity form using similarity variables and then solved using the 4^{th} order Runge - Kutta method. The key parameters such as the magnetic parameter, chemical reaction rate, variable fluid properties, unsteadiness, convection, and radiation parameter significantly affect flow behavior over an inclined plane. It was found that increasing the magnetic field strength enhances the fluid velocity, temperature, and concentration. Additionally, an increase in the unsteadiness variation parameter within the boundary layer leads to higher velocity and concentration while reducing temperature. Conversely, the fluid temperature and concentration decrease as the chemical reaction parameter in the boundary layer rises. Furthermore, an increase in the magnetic parameter results in increase in the heat transfer rate while simultaneously decreases the skin friction and mass transfer rates. Also, the fluid temperature decreases as radiation parameter increases.

Keywords: Unsteady flow; Convection; Variable fluid properties; Magnetic fields, Boundary layer flow.

Introduction

Studies on unsteady convection boundary layer flow with the presence of magnetic fields has attracted a great deal of interest because of its significance in the fields of research, technology and several manufacturing processes such as the fabrication of plastic sheets, solar power absorption and thermal energy storage (Vajravelu et al. 2013, Ahmed et al. 2021, and Raje et al. 2023).

Convection is the mechanism of heat transfer through a fluid in the presence of large fluid motion (Rana et al. 2012 and Zainal et al. 2021). It is important in industries and technical applications such as heating systems, air conditioning systems, cooling systems (car engines), refrigeration systems, chemical processes, and manufacturing processes (Das et al. 2015 and Khan et al. 2020). It plays a crucial role in controlling the temperature and flow of liquids and gases and is often used to transfer

heat and mass from one place to another (Olanrewaju et al. 2012 and Saqib et al. 2020). The heat transfer rate in convection process is determined by the fluid velocity, heat transfer, the fluid properties and the temperature difference between solid surface and the fluid (Alam et al. 2016 and Hussain et al. 2021). According to Hossain et al. (2017), convection is classified into two parties; namely natural (or free) and forced convection. Forced convection is the type of heat transfer in which a liquid or gas is made to flow over a solid surface by an external source such as pump or a fan. On the other hand, natural is the transfer of heat caused by the density difference in a fluid due to temperature variation. Convection can be observed in the boundary layer flow of the fluid adjacent to a solid surface.

The theory which describes boundary layer effects was first presented by Ludwing Prandtl in the early 1990's based on a fluid flow passed over solid surface (Schlichting 1979). Boundary layer is defined as a very thin layer of flowing fluid in contact with a surface in which the velocity of the fluid increases from zero at the surface to the free stream value of U_∞ (Schlichting 1979). According to Kitengeso et al. (2018), the layer making contact with the fixed sold surface comes to rest when the fluid touches it, and this situation is referred to as a 'no slip condition'. Since viscosity has the function of preventing fluid motion, the velocity on the surface decreases to zero, while the velocity of the fluid away from the solid surface increases to the free stream value of U_∞. According to Das et al. (2015), other features observed in the boundary layer are velocity and thermal boundary layers. According to James et al. (2015), the thickness of the boundary layer relies on a number of variables including temperature, the flow's type, viscosity, the solid surface's roughness, flow velocity and flow stability.

The study of MHD boundary layer flow over an electrically conducting liquid with a transverse magnetic field due to an expanding surface was first suggested by Pavlov in 1974. The theoretical study of the mutual interaction between the flow of electrically conductive liquids such as ionized gas, liquid metal and salt water (strong electrolytes) and magnetic fields is commonly known as Magnetohydrodynamic (MHD) (Pavlov, 1974). Electrically conducting liquids are used in power generators, electrostatic filter, MHD accelerators and thermal design exchanger (Nadeem et al. 2014). The combination of electromagnetic and hydrodynamic principles for continuous media forms the governing equations for magnetohydrodynamics. The MHD participation in an electrically conductive fluid leads to a resistance shaping force, which gives a resistance to motion of the fluid particle, which can be defined as the Lorentz force. The Lorentz force increases significantly with concentration and temperature rise of the liquids and therefore delays boundary layer detachment (Zainal et al. 2021).

Unsteady boundary layers arise as a result of various fluid flow scenarios, for example, the fluid is at rest and the body performs a periodic motion, or the body is at rest and the fluid performs a periodic motion (Schlichting, 1979 and Nazar et al. 2004). Different studies on unsteady boundary layer flow have been carried out by researchers such as Kumari and Nath 2010, Vajravelu et al. 2013, Ali et al. 2015, Reddy 2016, and Kitengeso et al. 2018. Their result shows that an increase in the transient parameter leads to a decrease in the thickness of velocity and thermal boundary layers, and there is a smooth transition from the steady to the transient state

Several studies have investigated the effects of magnetic fields on unsteady mixed convective boundary layer flow. For example, Ganopathirao and Ravindran (2015) investigated the non-uniform slot suction/injection into mixed convection MHD flow over a vertical wedge with chemical reaction, and found that the fluid flow velocity is decreasing by an increasing magnetic parameter. Alam et al. (2016) investigated the effects of variable fluid properties and thermophoresis on unsteady forced convection boundary flow along a

permeable stretching/shrinking wedge and discovered that the velocity, temperature, and concentration decrease as the unsteadiness parameter increases. Reddy (2016) investigated mass transfer effects on an unsteady MHD free convective flow of an incompressible viscous dissipative fluid past an infinite vertical porous plate. Sivasankaran et al. (2020) investigated the numerical simulation on convection of non-Newtonian fluid in a porous enclosure with non-uniform heating and thermal radiation, concluding that decreasing behavior of temperature is noticed by increasing the thermal radiation parameter. Megahed et al. (2021) examined the modelling of MHD fluid flow over an unsteady stretching sheet with thermal radiation, variable fluid properties and heat flux and discovered that the effect of radiation, unsteadiness, and the thermal conductivity is to increase both the local skin friction and nusselt number. Ahmed et al. (2021) and Reddy and Reddy (2022) investigated the thermal radiation effect on MHD unsteady with variable fluid properties, and found that heat transfer decreases with increasing the unsteadiness. All of the previous studies have not included both chemical reactions, radiation, magnetic fields, and variable fluid properties. Therefore, this study intends to extend the work of Kitengeso et al. (2018) by analyzing the unsteady convective boundary layer flow model with presence of Magnetic fields, chemical reaction, and radiation effect and variable fluid properties.

Materials and Methods

Consider the convective flow of viscous incompressible fluid under the influence of transverse magnetic field $\boldsymbol{B_o}$ past a vertical plate. The plate is inclined from the vertical with an acute angle γ measured in the clockwise direction as shown in Figure 1.

From Figure 1, choose the coordinate system such that x- axis is along the vertical plate and y- axis normal to the plate. The concentration and temperature of the ambient medium are C_∞ and T_∞, respectively. It is assumed that initially the fluid is at rest and that thermal conductivity and viscosity are temperature dependent. The fluid flow is characterized as unsteady, laminar, two dimensional, and in a state of local thermodynamic equilibrium. The fluid treated as an absorbing, gray, and radioactively emitting medium that does not scatter radiation. The Rosseland approximation is employed to describe the radioactive heat flux in the energy equation. Furthermore, the radiative heat flux in the x-direction is considered negligible in comparison with the y-direction. Also, it is assumed that there exists a homogeneous chemical reaction of first order with a constant rate k_1 on the boundary layer.

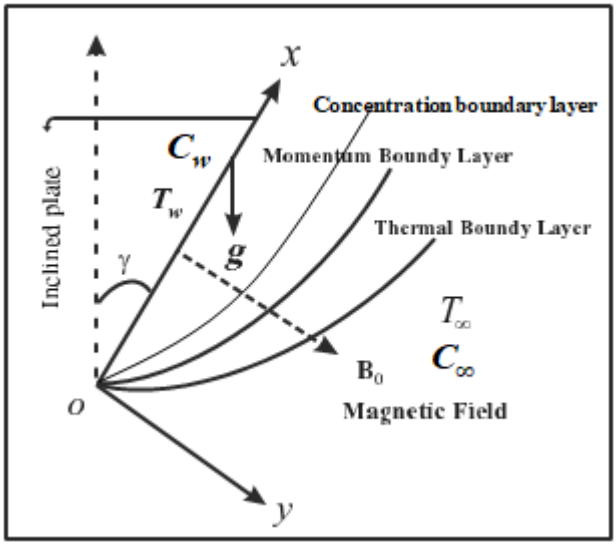

Figure 1: The physical model representation for fluid flow (Das et al. 2015).

Consider the schematic diagram for the fluid flow from Figure 1. The velocity vector is given as $\boldsymbol{u} = (u(x,y,t), v(x,y,t))$. The proposed model equation for the fluid under above conditions and assumptions is represented by the following nonlinear partial differential equations as,

$$\frac{\partial u}{\partial x} + \frac{\partial v}{\partial y} = 0 \qquad (1)$$

$$\left(\frac{\partial u}{\partial t} + u\frac{\partial u}{\partial x} + v\frac{\partial u}{\partial y}\right) = \left(\frac{\partial U}{\partial t} + U\frac{\partial U}{\partial x}\right) + g\beta(T - T_\infty)\cos(\gamma) + \frac{1}{\rho}\frac{\partial}{\partial y}\left(\mu(T)\frac{\partial u}{\partial y}\right) - \frac{\sigma B_0^2}{\rho}(u - U) \quad (2)$$

$$\rho C_\rho \left(\frac{\partial T}{\partial t} + u\frac{\partial T}{\partial x} + v\frac{\partial T}{\partial y}\right) = \frac{\partial}{\partial y}\left(k(T)\frac{\partial T}{\partial y}\right) + \mu(T)\left(\frac{\partial u}{\partial y}\right)^2 + \sigma B_o^2(u - U)^2 - \frac{\partial q_r}{\partial y} \qquad (3)$$

$$\frac{\partial C}{\partial t} + u\frac{\partial C}{\partial x} + v\frac{\partial C}{\partial y} = \frac{\partial}{\partial y}\left(D_m(T)\frac{\partial C}{\partial y}\right) - k_1(C - C_\infty) \qquad (4)$$

Following Kitengeso et al. (2018), the thermal conductivity $k(T)$ of fluid can vary linearly with temperature using a function

$$k(T) = k_\infty\left(1 + \frac{\epsilon}{\Delta T}(T - T_\infty)\right) \qquad (5)$$

And in terms of dimensionless, the temperature equation is reduced to the equation

$$k(\theta) = k_\infty(1 + \epsilon\theta) \qquad (6)$$

where k_∞ is the thermal conductivity of the fluid at free stream, $k(\theta)$ is the variation thermal conductivity with respect to dimensionless temperature, and ϵ is a small parameter that depends on the fluid's nature and it measures the rate of change of thermal conductivity with temperature.

On the other hand, the viscosity is considered to change exponentially with temperature (Mureithi 2014). In this case, the Arrhenius model which has an exponential shape is given as

$$\mu(T) = \mu_\infty e^{-\epsilon_o(T - T_\infty)} \qquad (7)$$

where μ_∞ is reference viscosity at reference temperature T_∞ and ϵ_o is a viscosity variation number which is defined as

$$\epsilon_o = \frac{1}{T_w - T_\infty} ln\left(\frac{\mu_\infty}{\mu_w}\right)$$

where μ_∞ is greater than μ_w, and μ_∞ and μ_w are fluid viscosity at free stream temperature, T_∞ and T_w respectively. For liquids ϵ_o is positive and for gases ϵ_o is negative (Mureithi, 2014).

Taylor expansion leads to a linear or inverse relationship of viscosity with temperature for small values of ϵ_o.
The diffusivity coefficient $D(T)$ of fluid can vary linearly with temperature using a function as

$$D(T) = D_\infty\left(1 + \frac{\epsilon_1}{\Delta T}(T - T_\infty)\right) \tag{8}$$

and in terms of dimensionless temperature the equation is reduced to the equation

$$D(\theta) = D_\infty(1 + \epsilon_1\theta) \tag{9}$$

where D_∞ is the diffusion coefficient of the fluid at free stream, $D(\theta)$ is the variation diffusion coefficient with respect to dimensionless temperature and ϵ_1 is a small parameter that depends on the fluid's nature and it measures the rate of change of chemical diffusivity with temperature.
The initial condition at $t = 0$ is given as

$$u(x, y, 0) = 0, v(x, y, 0) = 0, T(x, y, 0) = T_\infty, C(x, y, 0) = C_\infty \tag{10}$$

The boundary conditions for $t > 0$ are

$$\begin{cases} u(x, 0, t) = 0, \quad v(x, 0, t) = 0, T(x, 0, t) = T_w, C(x, 0, t) = C_w \ \ at\ y = 0 \\ u(x, \infty, t) = U, v(x, \infty, t) = 0, T(x, \infty, t) = T_\infty, C(x, \infty, t) = C_\infty \ \ as\ y \longrightarrow \infty \end{cases} \tag{11}$$

The radiative heat flux can be expressed by Rosseland approximation by Brewster as

$$q_r = \frac{4\sigma^*}{3k^*}\frac{\partial T^4}{\partial y} \tag{12}$$

where σ^* and k^* are the stephan-Boltzman constant and mean absorption coefficient. Assume that the temperature difference within the flow is such that the term T^4 can be expressed as a linear function of temperature. Hence expanding T^4 in a Tylor series about T_∞ and neglecting higher-order term obtain $T^4 \approx 4T_\infty^3 T - T_\infty^3$ (Vajravelu et al 2013).
Introducing the stream function (ψ) such that

$$u = \frac{\partial \psi}{\partial y},\ v = -\frac{\partial \psi}{\partial x}, \tag{13}$$

the continuity equation (1) is satisfied identically. The following similarity transformation equations have been used to transform equations (2-4) together with boundary conditions (11) from dimensional to dimensionless equations.

$$u(x, y, t) = U(x, y)h(\eta), \quad T(x, y, t) = T_\infty + (T_w - T_\infty)\theta(\eta)$$
$$\eta = \frac{y}{G(x,y)}, \quad C(x, y, t) = C_\infty + (C_w - C_\infty)\phi(\eta)$$

where y coordinate relates to the boundary layer similarity variable, since the dimensionless scale $G(x, t)$ is related to boundary layer growth and η is the boundary layer similarity variable (Sattar 2013).

$$G(x, t) = \sqrt{\left(\frac{2}{n+1}\right)}\frac{vx}{U(x,t)}, \quad (x, y, t) = y\sqrt{U\left(\frac{x,y}{vx}\right)\left(\frac{n+1}{2}\right)}$$
$$\eta = y\sqrt{\left(\left(\frac{n+1}{2}\right)\left(\frac{U(x,t)}{vx}\right)\right)}, \quad U(x, t) = Z\left(\frac{x}{t}\right)^n, \psi(x, y, t) = \sqrt{\left(\left(\frac{2}{n+1}\right)vxU(x, t)\right)}f(\eta)$$

The angle of the inclined plate $y = \pi H$ is related to *n* through the expression $n = \frac{\gamma}{\pi}$ (Kitengeso et al. 2018). Thus, if $n = 0\ and\ 1$ it corresponds to the plate at an angle $\gamma = 0\ and \frac{\pi}{2}$ respectively, which is vertically. When $n = 0.5$ the flow is correspond to the stagnation at a horizontal plate. The ordinary differential equation with respect to η becomes

$$\begin{aligned} f''' = \alpha\theta' f'' - \left(\frac{2}{n+1}\right)\lambda e^{\alpha\theta}\theta\cos(\gamma) + \left(\frac{1}{n+1}\right)Ste^{\alpha\theta}(1 - f' - \eta f'') \\ + \frac{2n}{n+1}e^{\alpha\theta}((f')^2 - 1) - e^{\alpha\theta}ff'' \\ + \left(\frac{2}{n+1}\right)Me^{\alpha\theta}(f' - 1) \end{aligned} \tag{14}$$

$$(1+\varepsilon\theta+P_rRd)\theta'' = -\left(\frac{1}{n+1}\right)StP_r\eta\theta' - P_r\theta' f - \varepsilon(\theta')^2 - P_rE_ce^{-\alpha\theta}(f'')^2 - \left(\frac{2}{n+1}\right)MP_rE_c(f'-1)^2 \quad (15)$$

$$(1+\epsilon_1\theta)\phi'' = \left(\frac{1}{n+1}\right)StS_c\eta\phi' - S_cf\phi' - \varepsilon_1\theta'\phi' + \left(\frac{2}{n+1}\right)S_ck_r\phi \quad (16)$$

Subjected to the boundary conditions

$$\begin{cases} f'(\eta=0)=0, f(\eta=0)=0, \theta(\eta=0)=1, \phi(\eta=0)=1 \\ f(\eta\to\infty)=1, \quad \theta(\eta\to\infty)=0, \quad \phi(\eta\to\infty)=0 \end{cases} \quad (17)$$

Where $\lambda=\frac{Gr_x}{Re_x}$ is the convection parameter, $St=\frac{x}{tU}$ is unsteady parameter, $M=\frac{\sigma x\beta_o^2}{\rho U}$ is the magnetic parameter,$E_c=\frac{U^2}{\Delta TC_p}$is the Eckert number,$S_c=\frac{\nu}{D_\infty}$ is the Schmidt number, $P_r=\frac{\mu_\infty C_p}{k_\infty}$ is the prandlt number,$k_r=\frac{xk_1}{U(x,t)}$ is the chemical reaction, and $Rd=\frac{16\sigma_oT_\infty^3}{3k_ok_\infty}$ is the Radiation parameter.

For the type of boundary layer flow consideration, the physical quantities of interest are the local Sherwood number Sh_x, local skin friction coefficient C_f, and local Nusselt number Nu_x.

$$Sh_x(Re_x)^{-\frac{1}{2}} = -(1+\varepsilon_1)\sqrt{\tfrac{n+1}{2}}\phi'(0), C_f(Re_x)^{\frac{1}{2}} = e^{-\alpha}\sqrt{2(n+1)}f''(0), Nu_x(Re_x)^{-\frac{1}{2}} = -(1+\epsilon)\sqrt{\tfrac{n+1}{2}\theta'(0)}$$

Numerical simulation of the boundary layer

The equations (14-16) are nonlinear and are solved by converting them into first order ordinary differential equations and treating them as initial value problems. The initial value problems are numerically solved by using a standard initial value solver, namely the Shooting method together with Runge-Kutta integration scheme. This can be done as follows,

Suppose $f_1=f,\ f_2=f',\ f_3=f'',\ f_4=\theta, f_5=\theta',\ f_6=\phi,\ f_7=\phi'$ $f_6=\phi$, and the corresponding derivatives of the above relationship becomes

$$f_1'=f', \quad f_2'=f'', \quad f_3'=f''', \quad f_4'=\theta', \quad f_5'=\theta'', \quad f_6'=\phi', \quad f_7'=\phi''$$

Using these relationships, the equations (14-16) are simplified and are written as the first order ordinary differential equations with respect to η as follows.

$$f_1' = f_2, \quad (18)$$

$$f_2' = f_3, \quad (19)$$

$$f_3' = \alpha f_5f_3 - \left(\frac{2}{n+1}\right)\lambda e^{\alpha f_4}f_4\cos(\gamma) + \left(\frac{1}{n+1}\right)Ste^{\alpha f_4}(1-f_2-\eta f_3) + \frac{2n}{n+1}e^{\alpha f_4}((f_2)^2-1) - e^{\alpha f_4}f_1f_3 + \left(\frac{2}{n+1}\right)Me^{\alpha f_4}(f_2-1), \quad (20)$$

$$f_4' = f_5, \quad (21)$$

$$f_5' = -\left(\frac{1}{n+1}\right)StP_r\eta f_5 - P_rf_5f_1 - \varepsilon(f_5)^2 - P_rE_ce^{-\alpha f_4}(f_3)^2 - \left(\frac{2}{n+1}\right)MP_rE_c(f_2-1)^2/(1+\varepsilon f_4+P_rRd), \quad (22)$$

$$f_6' = f_7, \quad (23)$$

$$f_7' = \left(\frac{1}{n+1}\right)StS_c\eta f_7 - S_cf_1f_7 - \varepsilon_1f_5f_7 + \left(\frac{2}{n+1}\right)S_ck_rf_6/(1+\epsilon_1f_4), \quad (24)$$

Subjected to the boundary conditions

$$\begin{cases} at\ \ \eta = 0 & f_1' = f_2 = 0,\ \ f_1 = 0,\ \ f_4 = 1,\ \ f_6 = 1 \\ As\ \ \eta \to \infty & f_1' = f_2 = 1, \quad f_4 = 0,\ \ f_6 = 0 \end{cases} \tag{25}$$

Results

The system of nonlinear ordinary differential equations with boundary conditions are solved numerically using the bvp4c with MATLAB based on the Runge-Kutta 4^{th} order method. The non-dimensional parameters which are being investigated are the thermal conductivity variation parameter $\boldsymbol{\epsilon}$, variable diffusion coefficient parameter ϵ_1, the Magnetic parameter $\boldsymbol{M}$, the Prandtl number $\boldsymbol{P_r}$, the Radiation parameter **Rd**, the unsteady parameter ***St,*** the aligned angle $\boldsymbol{\gamma}$, convection parameter $\boldsymbol{\lambda}$ and chemical reaction parameter $\boldsymbol{k_r}$. These parameters have influence on the velocity, concentration, reduced Nusselt number $\boldsymbol{Nu_x(Re_x)^{-\frac{1}{2}}}$, reduced Sherwood number $\boldsymbol{Sh_x(Re_x)^{-\frac{1}{2}}}$, local skin friction $\boldsymbol{C_f(Re_x)^{\frac{1}{2}}}$ and temperature on the boundary layer. The numerical computations for these parameters are carried out for $0.1 \leq \boldsymbol{\epsilon} \leq \boldsymbol{0.7}$, $0.5 \leq \boldsymbol{M} \leq \boldsymbol{3}, 0 \leq \boldsymbol{St} \leq \boldsymbol{0.5}, 0.72 \leq \boldsymbol{P_r} \leq \boldsymbol{2}, 0.5 \leq \boldsymbol{\lambda} \leq \boldsymbol{1.5}, 0.1 \leq \boldsymbol{k_r} \leq \boldsymbol{1}, 0 \leq \boldsymbol{\gamma} \leq \boldsymbol{\pi}, 0 \leq \boldsymbol{\epsilon_1} \leq \boldsymbol{0.5}$ and $0 \leq \boldsymbol{Rd} \leq \boldsymbol{5}$**.** The step size $\Delta\eta = 0.1$ has been used in the analysis, where$0 \leq \eta \leq 6$ and the accuracy of 10^{-8} was used as stopping criteria. The influence of these parameters on the skin friction coefficient, the local Nusselt number, the velocity, temperature and concentration boundary layers, have been presented through graphically.

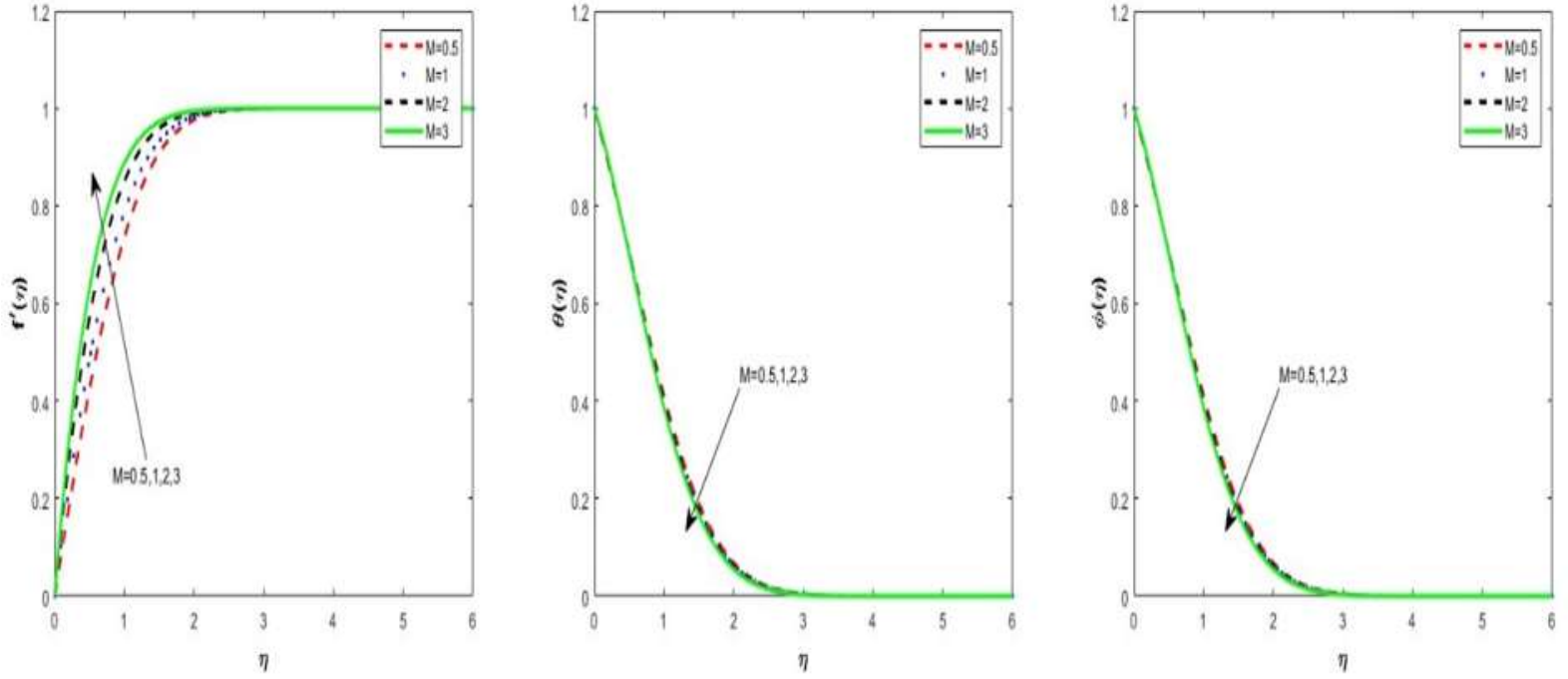

(a) Velocity $f'(\eta)$ (b) temperature$\theta(\eta)$ (c) concentration $\phi(\eta)$

Figure 2: Effects of varying magnetic parameter **M** on, (a) velocity $f'(\eta)$, (b) temperature$\theta(\eta)$, (c) concentration$\phi(\eta)$ with $\alpha = 0.2, \boldsymbol{\lambda = 0.5}, \boldsymbol{\gamma = \frac{2\pi}{3}}, \boldsymbol{n = 0.5}, \boldsymbol{St = 1}, \boldsymbol{E_c = 0.2}, \boldsymbol{P_r = 0.72}, \boldsymbol{\epsilon_1 = 0.01}, \boldsymbol{\epsilon = 0.2}, \boldsymbol{Rd = 0.1}, \boldsymbol{S_c = 0.1}$ and $\boldsymbol{k_r = 0.1}$

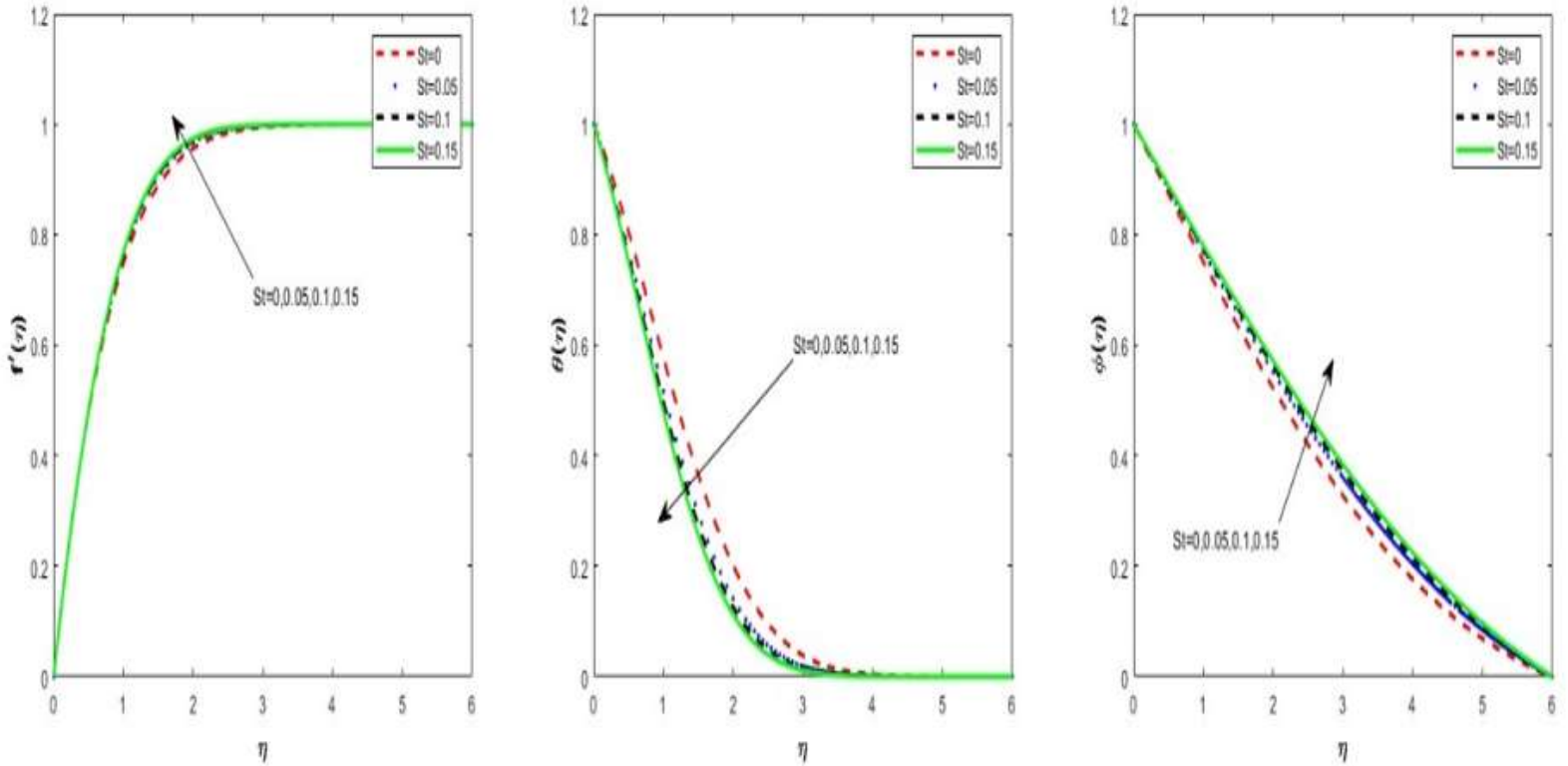

(a) Velocity $f'(\eta)$ (b) temperature $\theta(\eta)$ (c) concentration $\phi(\eta)$

Figure 3: Effects of varying unsteady parameter **St** on, (a) velocity $f'(\eta)$, (b) temperature $\theta(\eta)$, (c) concentration $\phi(\eta)$ with $\alpha = 0.2, \boldsymbol{\lambda} = \mathbf{0.5}, \boldsymbol{\gamma} = \frac{\mathbf{2\pi}}{\mathbf{3}}, \boldsymbol{n} = \mathbf{0.5}, \boldsymbol{M} = \mathbf{1}, \boldsymbol{E_c} = \mathbf{0.2}, \boldsymbol{P_r} = \mathbf{0.72}, \boldsymbol{\epsilon_1} = \mathbf{0.01}, \boldsymbol{\epsilon} = \mathbf{0.2}, \boldsymbol{Rd} = \mathbf{0.1}, \boldsymbol{S_c} = \mathbf{0.1}$ and $\boldsymbol{k_r} = \mathbf{0.1}$

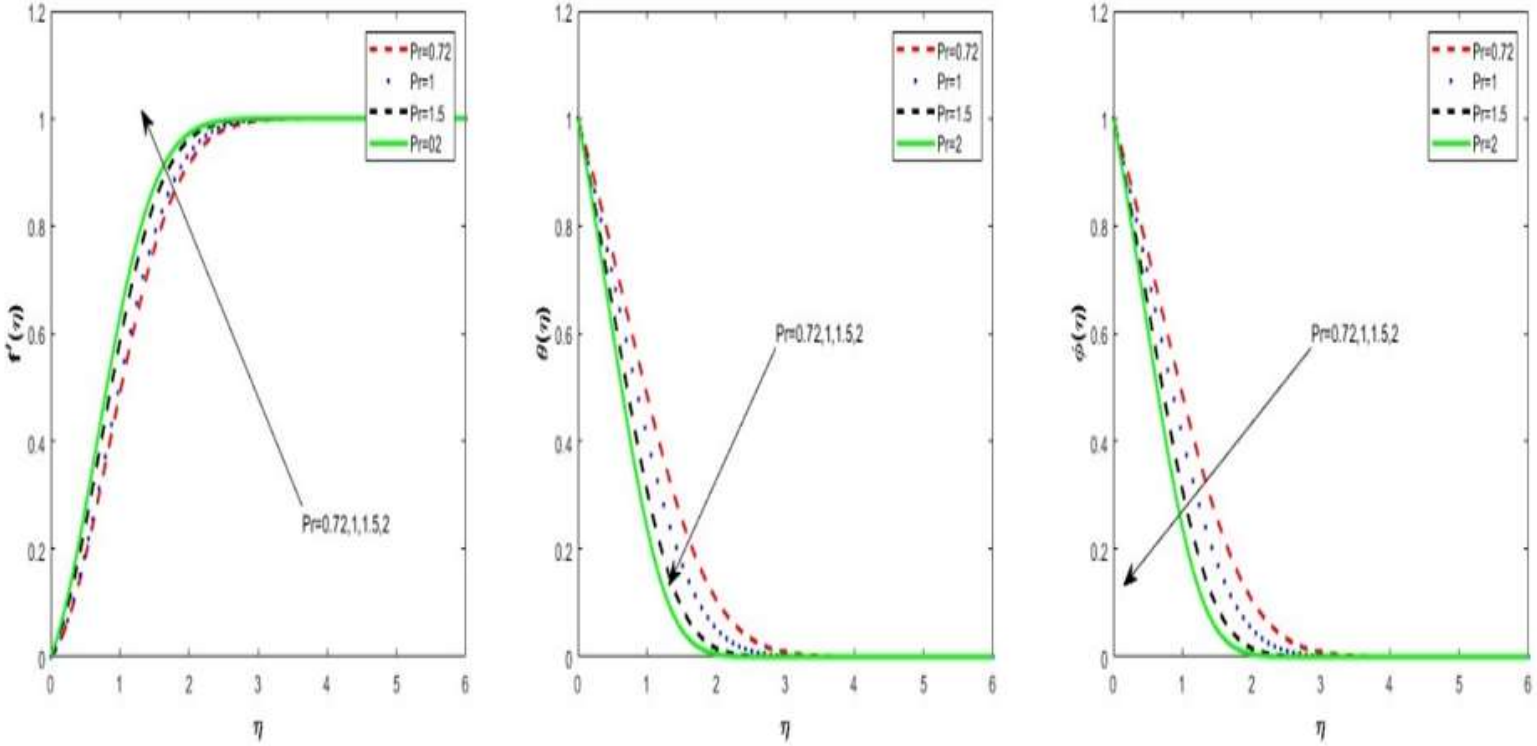

(a) Velocity $f'(\eta)$ (b) temperature $\theta(\eta)$ (c) concentration $\phi(\eta)$

Figure 4: Effects of varying prandlt number parameter $\boldsymbol{P_r}$ on, (a) velocity $f'(\eta)$, (b) temperature$\theta(\eta)$, (c) concentration$\phi(\eta)$ with $\alpha = 0.2, \boldsymbol{\lambda} = \boldsymbol{0.5}, \boldsymbol{\gamma} = \frac{\boldsymbol{2\pi}}{\boldsymbol{3}}, \boldsymbol{n} = \boldsymbol{0.5}, \boldsymbol{M} = \boldsymbol{1}, \boldsymbol{E_c} = \boldsymbol{0.2}, \boldsymbol{k_r} = \boldsymbol{0.1}, \boldsymbol{\epsilon_1} = \boldsymbol{0.01}, \boldsymbol{\epsilon} = \boldsymbol{0.2}, \boldsymbol{Rd} = \boldsymbol{0.1}, \boldsymbol{S_c} = \boldsymbol{0.1}$ and $\boldsymbol{St} = \boldsymbol{1}$.

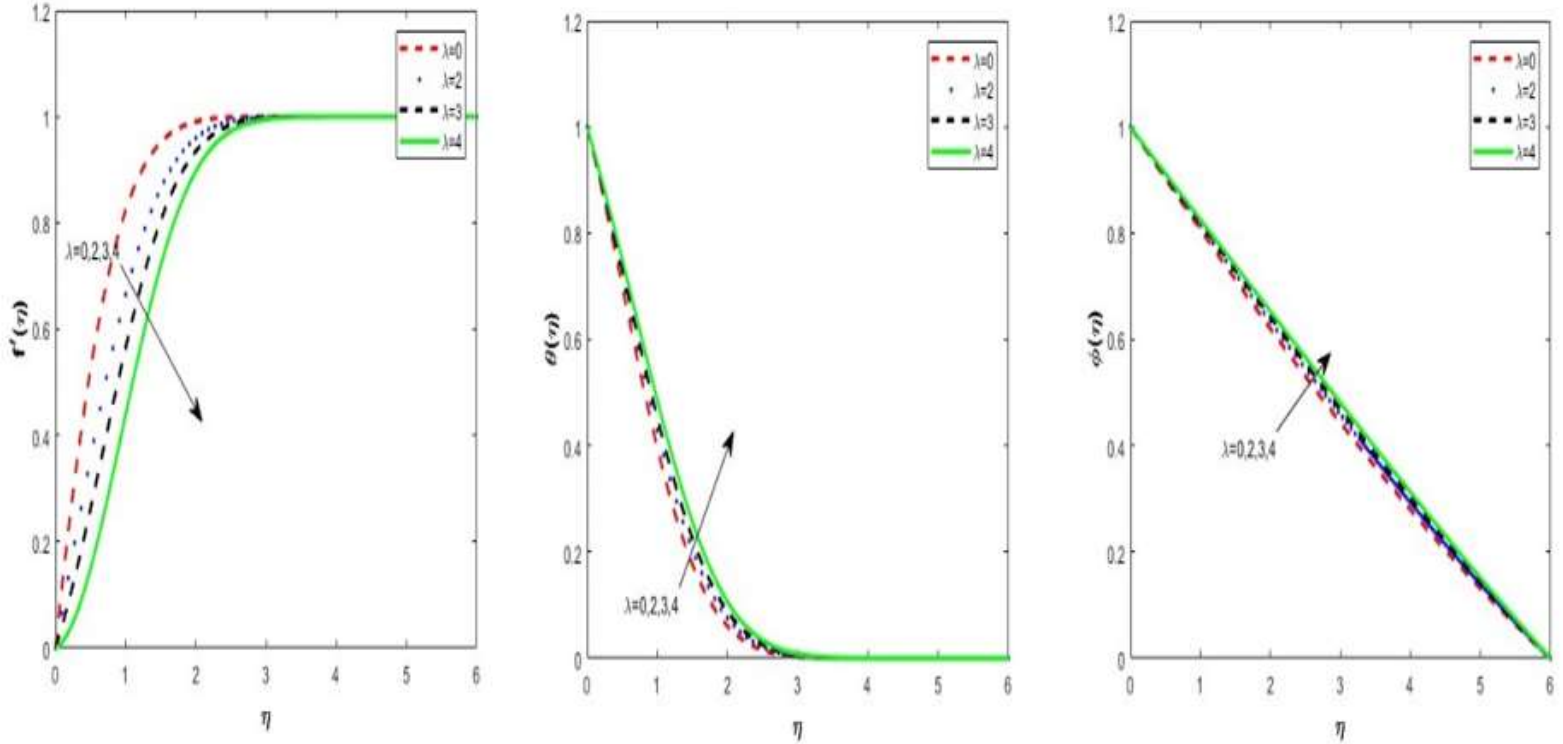

(a) Velocity $f'(\eta)$ (b) temperature $\theta(\eta)$ (c) concentration $\phi(\eta)$

Figure 5: Effects of varying convection parameter $\boldsymbol{\lambda}$ on, (a) velocity $f'(\eta)$, (b) temperature $\theta(\eta)$, (c) concentration $\phi(\eta)$ with $\alpha = 0.2, \boldsymbol{St} = \mathbf{1}, \boldsymbol{\gamma} = \frac{\boldsymbol{2\pi}}{\mathbf{3}}, \boldsymbol{n} = \mathbf{0.5}, \boldsymbol{M} = \mathbf{1}, \boldsymbol{E_c} = \mathbf{0.2}, \boldsymbol{P_r} = \mathbf{0.72}, \boldsymbol{\epsilon_1} = \mathbf{0.01}, \boldsymbol{\epsilon} = \mathbf{0.2}, \boldsymbol{Rd} = \mathbf{0.1}, \boldsymbol{S_c} = \mathbf{0.1}$ and $\boldsymbol{k_r} = \mathbf{0.1}$

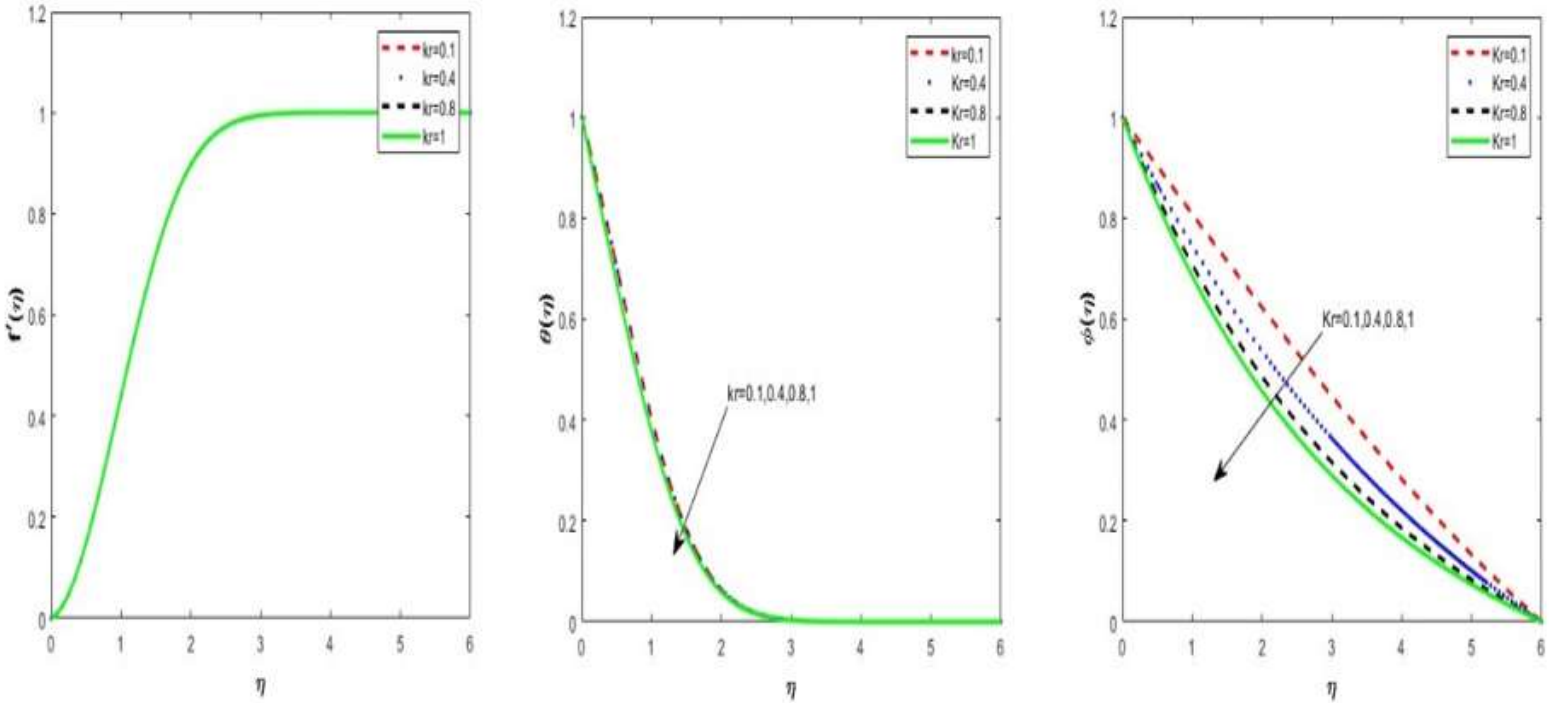

(a) Velocity $f'(\eta)$ (b) temperature $\theta(\eta)$ (c) concentration $\phi(\eta)$

Figure 6: Effects of varying chemical reaction parameter $\boldsymbol{k_r}$ on, (a) velocity $f'(\eta)$, (b) temperature $\theta(\eta)$, (c) concentration $\phi(\eta)$ with $\alpha = 0.2, \boldsymbol{\lambda = 0.5}, \boldsymbol{\gamma = \frac{2\pi}{3}}, \boldsymbol{n = 0.5}, \boldsymbol{M = 1}, \boldsymbol{E_c = 0.2}, \boldsymbol{P_r = 0.72}, \boldsymbol{\epsilon_1 = 0.01}, \boldsymbol{\epsilon = 0.2}, \boldsymbol{Rd = 0.1}, \boldsymbol{S_c = 0.1}$ and $\boldsymbol{St = 1}$

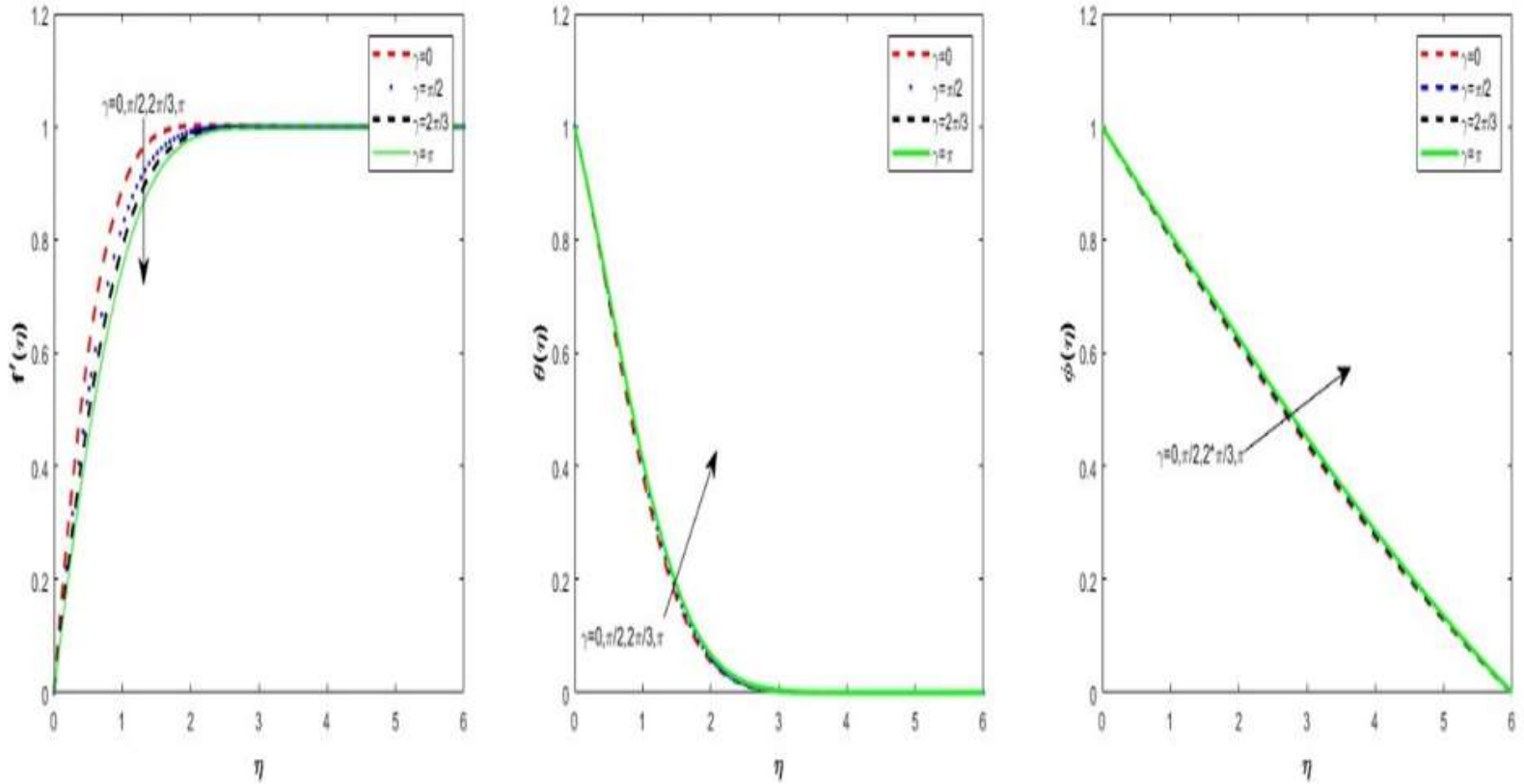

(a) Velocity $f'(\eta)$ (b) temperature $\theta(\eta)$ (c) concentration $\phi(\eta)$

Figure 7: Effects of varying angle parameter $\boldsymbol{\gamma}$ on, (a) velocity $f'(\eta)$, (b) temperature $\theta(\eta)$, (c) concentration$\phi(\eta)$ with $\alpha = 0.2, \boldsymbol{\lambda = 0.5, St = 1, n = 0.5, M = 1, E_c = 0.2, P_r = 0.72, \epsilon_1 = 0.01, \epsilon = 0.2, Rd = 0.1, S_c = 0.1}$ and $\boldsymbol{k_r = 0.1}$

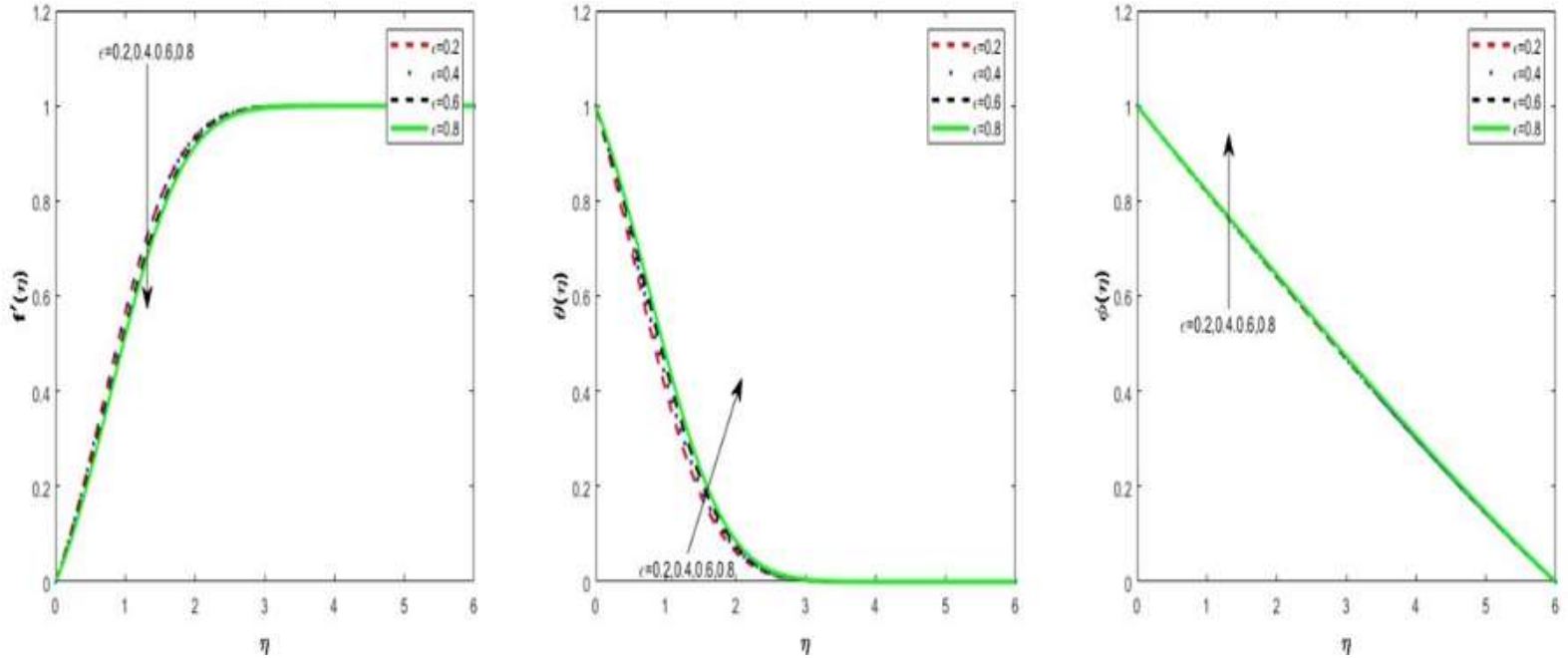

(a) Velocity $f(\eta)$ (b) temperature $\theta(\eta)$ (c) concentration $C(\eta)$

Figure 8: Effects of varying thermal conductivity parameter $\boldsymbol{\epsilon}$ on, (a) velocity $f'(\eta)$, (b) temperature $\theta(\eta)$, (c) concentration $\phi(\eta)$ with $\alpha = 0.2, \boldsymbol{\lambda = 0.5}, \boldsymbol{\gamma = \frac{2\pi}{3}}, \boldsymbol{n = 0.5}, \boldsymbol{M = 1}, \boldsymbol{E_c = 0.2}, \boldsymbol{P_r = 0.72}, \boldsymbol{\epsilon_1 = 0.01}, \boldsymbol{St = 1}, \boldsymbol{Rd = 0.1}, \boldsymbol{S_c = 0.1}$ and $\boldsymbol{k_r = 0.1}$

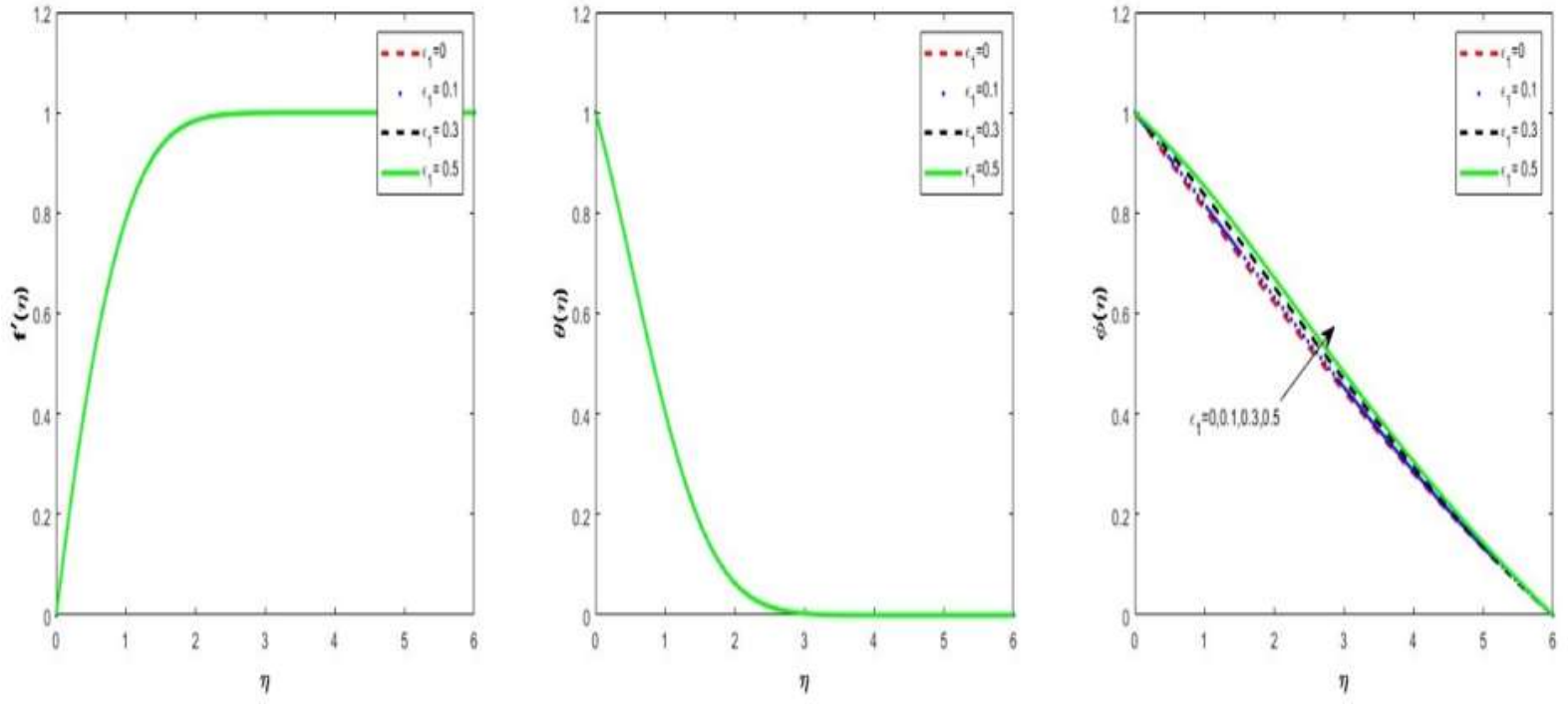

(a) Velocity $f;(\eta)$ (b) temperature $\theta(\eta)$ (c) concentration $\phi(\eta)$

Figure 9: Effects of varying variable diffusion parameter $\boldsymbol{\epsilon_1}$ on, (a) velocity $f'(\eta)$, (b) temperature$\theta(\eta)$, (c) concentration$\phi(\eta)$ with $\alpha = 0.2, \boldsymbol{\lambda} = \mathbf{0.5}, \boldsymbol{\gamma} = \frac{\mathbf{2\pi}}{\mathbf{3}}, \boldsymbol{n} = \mathbf{0.5}, \boldsymbol{M} = \mathbf{1}, \boldsymbol{E_c} = \mathbf{0.2}, \boldsymbol{P_r} = \mathbf{0.72}, \boldsymbol{St} = \mathbf{1}, \boldsymbol{\epsilon} = \mathbf{0.2}, \boldsymbol{Rd} = \mathbf{0.1}, \boldsymbol{S_c} = \mathbf{0.1}$ and $\boldsymbol{k_r} = \mathbf{0.1}$

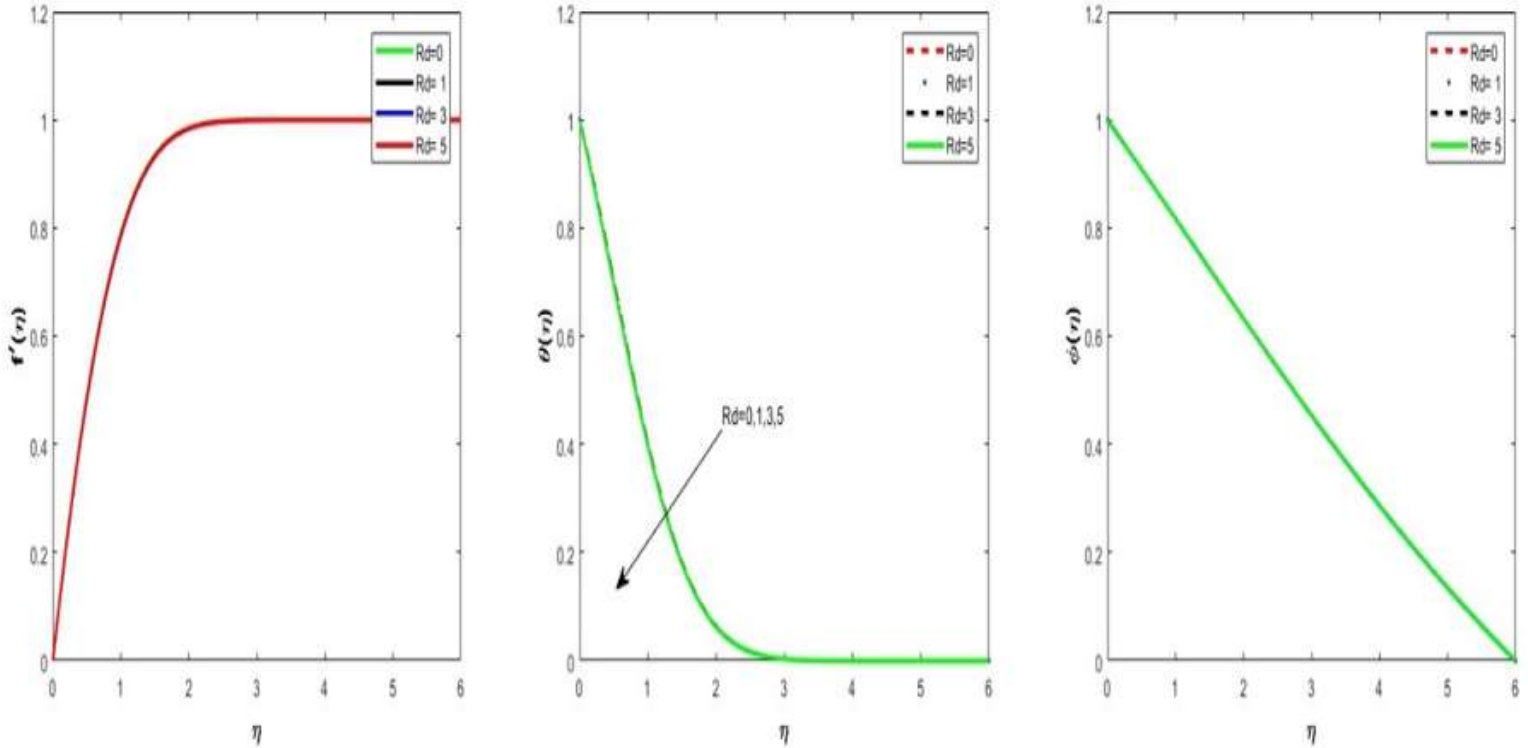

(a) velocity $f'(\eta)$ (b) temperature $\theta(\eta)$ (c) concentration $\phi(\eta)$

Figu re 10: Effects of varying radiation parameter Rd on, (a) velocity $f'(\eta)$, (b) temperature $\theta(\eta)$, (c) concentration $\phi(\eta)$ with $\alpha = 0.2, \boldsymbol{\lambda} = \mathbf{0.5}, \boldsymbol{\gamma} = \frac{\mathbf{2\pi}}{\mathbf{3}}, \boldsymbol{n} = \mathbf{0.5}, \boldsymbol{M} = \mathbf{1}, \boldsymbol{E_c} = \mathbf{0.2}, \boldsymbol{P_r} = \mathbf{0.72}, \boldsymbol{\epsilon_1} = \mathbf{0.01}, \boldsymbol{\epsilon} = \mathbf{0.2}, \boldsymbol{St} = \mathbf{1}, \boldsymbol{S_c} = \mathbf{0.1}$ and $\boldsymbol{k_r} = \mathbf{0.1}$

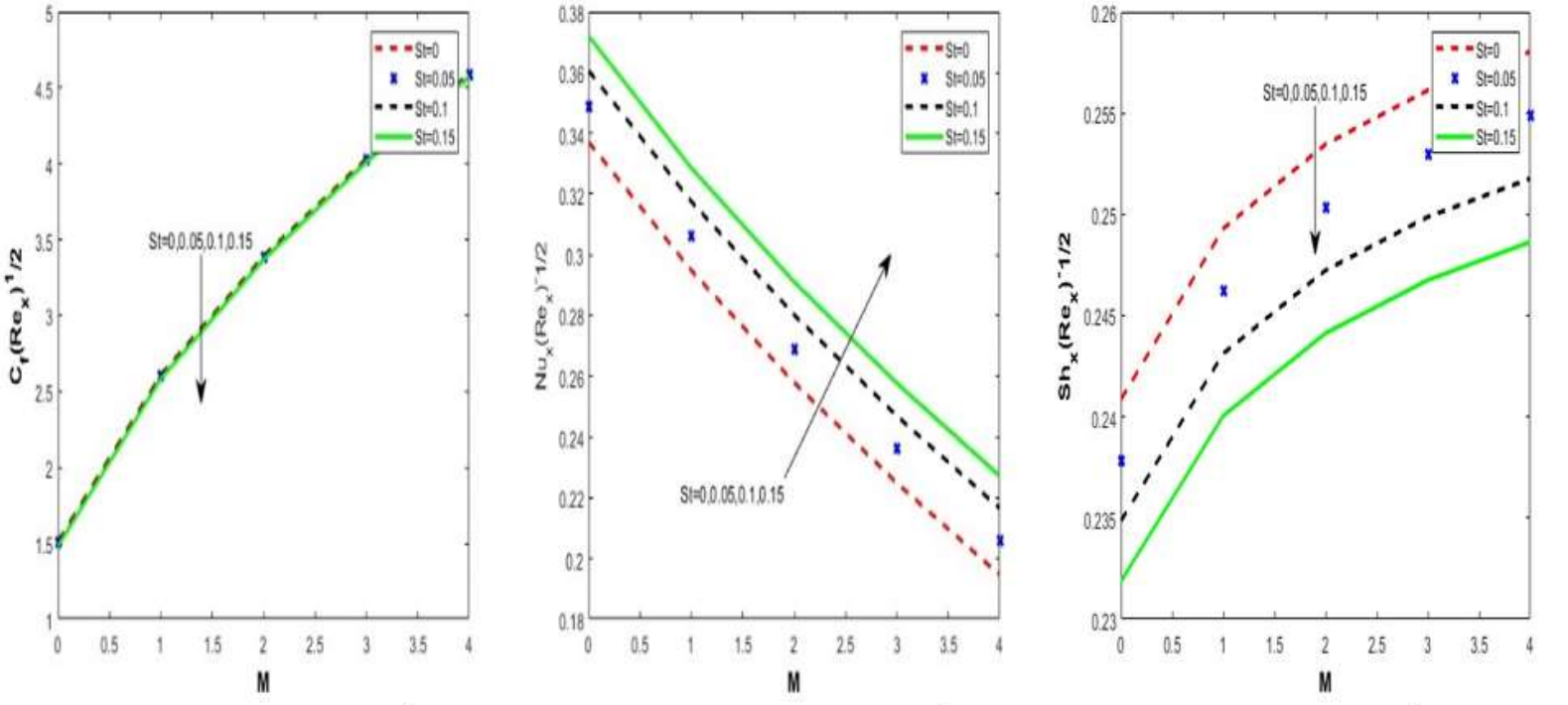

(a) Skin friction $C_f(Re_x)^{\frac{1}{2}}$	(b) Nusselt number $Nu_x(Re_x)^{-\frac{1}{2}}$,	(c) Sherwood $Sh_x(Re_x)^{-\frac{1}{2}}$

Figure 11: Effects of varying magnetic M and unsteady St parameters on, (a) Skin friction coefficient $C_f(Re_x)^{\frac{1}{2}}$, (b) Nusselt number $Nu_x(Re_x)^{-\frac{1}{2}}$, (c) Sherwood number $Sh_x(Re_x)^{-\frac{1}{2}}$,with $\alpha = 0.2, \boldsymbol{\lambda = 0.5}, \boldsymbol{\gamma = \frac{2\pi}{3}}, \boldsymbol{n = 0.5}, \boldsymbol{M = 1}, \boldsymbol{E_c = 0.2}, \boldsymbol{P_r = 0.72}, \boldsymbol{\epsilon_1 = 0.01}, \boldsymbol{\epsilon = 0.2}, \boldsymbol{Rd = 0.1}, \boldsymbol{S_c = 0.1}$ and $\boldsymbol{k_r = 0.1}$

Discussion

Figures 2(a), (b), and (c) show the effect of varying the Magnetic parameter $\boldsymbol{M}$ on velocity $f'(\eta)$, temperature $\theta(\eta)$, and concentration $\phi(\eta)$, respectively. The velocity of the liquid in the boundary layer increases as the value of the magnetic parameter increases. This is because the Lorentz force opposes the viscous forces, resulting in a thin velocity boundary layer. The temperature and concentration of the fluid decrease, as the magnetic parameter increases as expected due to the Lorentz force. This is similar to a drag force that tends to oppose the flow of liquid, thus reducing the temperature and concentration of the liquid. As the magnetic parameter increases, the thickness of the boundary layer also decreases.

Figures 3(a), (b), and (c) show the effect of varying the unsteady parameter $\boldsymbol{St}$ on velocity $f'(\eta)$, temperature $\theta(\eta)$, and concentration $\phi(\eta)$, respectively. It is observed that the fluid's temperature profiles decrease as unsteady parameter increases. The thermal boundary layer typically thickens with increasing steadiness. While the flow velocities and concentration increases as unsteady flow increase.

Figures 4(a), (b), and (c) show the effect of varying the Prandtl parameter $\boldsymbol{P_r}$ on velocity $f'(\eta)$, temperature $\theta(\eta)$, and concentration $\phi(\eta)$, respectively. Prandtl number is defined as the ratio between the momentum diffusivity and thermal diffusivity. It can be noted that an increase in the prandtl number leads to a decrease in the temperature and concentration. These figures also demonstrate how a decrease in Prandtl number causes the thermal boundary layer thickness to rise sharply. This is due to the fluid's high conductivity at low Prandtl number values. Physically, an increase in Prandtl parameter causes a decrease in thermal diffusivity, which in turn causes a decrease in the capacity to transfer energy by conduction, hence a reduction in the thermal boundary layer and increasing the velocity.

Figures 5(a), (b), and (c) show the effect of varying the convection parameter $\boldsymbol{\lambda}$ on velocity $f'(\eta)$, temperature $\theta(\eta)$, and concentration $\phi(\eta)$, respectively. When the mixed convection parameter is increased, the fluid temperature and concentration in the boundary layer also increases. This is because increasing values of convection parameter induce natural convection flow and reduce forced convection flow, which in turn causes temperature and concentration to increase. The velocity changes very smoothly within boundary layer as convection parameter increases.

Figures 6(a), (b), and (c) show the effect of varying the chemical reaction parameter $\boldsymbol{k_r}$ on velocity $f'(\eta)$, temperature $\theta(\eta)$, and concentration $\phi(\eta)$, respectively. It is clear from temperature and concentration that as the chemical reaction parameter increases, the temperature and concentration profile decreases; that is, the chemical reaction parameter is a retarding agent that causes the temperature and concentration in the boundary layer to decrease, and thus the solute boundary layer turns out to be thinner at a point very close to the plate and increases mass transfer.

Figures 7(a), (b), and (c) show the effect of varying the angle parameter $\boldsymbol{\gamma}$ on velocity $f'(\eta)$, temperature $\theta(\eta)$, and concentration $\phi(\eta)$, respectively. It was observed that if the angle of slope increases counterclockwise from the vertical axis, the speed of fluids decreases. This is due to the fact that as the tilt angle increases, it causes both the concentration and the temperature to decrease, and thus the effect of thermal buoyancy on the fluid decreases and finally limits the cooling process. This is due to the decrease in gravity.

Figures 8(a), (b), and (c) show the effect of varying the thermal conductivity parameter $\boldsymbol{\epsilon}$ on velocity $f'(\eta)$, temperature $\theta(\eta)$, and concentration $\phi(\eta)$, respectively. It can be noted that the temperature and concentration tend to increase as the variable thermal conductivity parameter increases. This is due to the increase in thermal boundary layer thickness; its effect is higher at the boundary layer and decreases as you approach the free stream.

Figures 9(a), (b), and (c) show the effect of varying variable diffusion coefficient

parameters ϵ_1 on velocity $f'(\eta)$, temperature $\theta(\eta)$, and concentration $\phi(\eta)$, respectively. Since the diffusion coefficient is a linear function of temperature, the concentration tends to increase as temperature rises along with the diffusion coefficient. This is because the diffusion coefficient is highly dependent on the concentration gradient, as demonstrated by Fick's law of concentration. Therefore, the concentration increases as variable diffusion coefficient parameter increases.

Figures 10(a), (b), and (c) show the effect of varying thermal radiation parameters ***Rd*** on velocity $f'(\eta)$, temperature $\theta(\eta)$, and concentration $\phi(\eta)$, respectively. The temperature distribution in the flow region decreases as radiation parameter increases because, in general, the presence of chemical reactions produces generations of radiative heat flux. As a result, an increase in radiation parameter causes the boundary layer thickness to decrease and the surface heat transfer rate to improve, while in the velocity and concentration, there is no effect observed.

Figure 11(a) shows the effects of magnetic parameter **M** and unsteady Parameter ***St*** on skin friction Coefficient $C_f(Re_x)^{\frac{1}{2}}$. As the mixed convection parameter rises, skin friction at the inclined plate's surface increases. This is due to the fact that, the fluid velocity in the boundary layer increases as the convection parameter values rise. As the unsteady parameter rises, skin friction falls, as Figure 11(a) illustrates.

Figure 11(b) shows the effects of magnetic parameter **M** and unsteady parameter ***St*** on Nusselt number $Nu_x(Re_x)^{-\frac{1}{2}}$. As the convection parameter increases, the Nusselt number at the inclined plate's surface decreases. This is due to the fact that, as the figure 11(b) shows, the fluid temperature in the boundary layer drops as the convection parameter values increase. As the unsteady parameter rises, the Nusselt number rises also.

Figure 11(c) shows the effects of magnetic parameter **M** and unsteady parameter ***St*** on skin friction Coefficient $Sh_x(Re_x)^{-\frac{1}{2}}$. As the convection parameter rises, Sherwood number at the inclined plate's surface increases. This is due to the fact that the fluid concentration in the boundary layer increases as the convection parameter values rise. As the unsteady parameter rises, the Sherwood number falls, as Figure 11(c) illustrates.

Conclusion

An unsteady convective boundary layer flow model with the presence of magnetic fields and temperature dependent properties over the inclined plate was investigated and analyzed using fourth order Runge-Kutta integration. The effects of unsteadiness, magnetic fields, reaction rate parameters, radiation, convection, and variable fluid properties over the inclined plate were discussed and presented in graphical forms. It was observed that an increase in magnetic parameters results in an increase in velocity and a decrease in temperature and concentration within the boundary layer. Both temperature and concentration increased in the boundary layer by increasing the thermal conductivity parameter. An increase in the variable diffusion coefficient parameter causes the concentration to increase. The increase in the unsteadiness parameter results in an increase in velocity and a decrease in the temperature and concentration. The increase in the reaction rate parameter results in a decrease in temperature and concentration. Furthermore, the skin friction coefficient, rate of heat transfer (reduced Nusselt number), and rate of mass transfer (reduced Sherwood number) were enhanced on the surface of the plate by increasing the convection parameters and magnetic parameters. The rate of heat transfer (reduced Nusselt number) at the surface of the plate decreases with the increase in convection parameter, while both the skin friction coefficient and reduced Sherwood number increase.

The goal of this study was to conduct a theoretical investigation and analysis that would serve as a foundation for upcoming experimental work. Additionally, research into the effects of injection and suction with slip conditions on a flow over a permeable surface can be done in the future.

Acknowledgement

I would like to thank the Institution of Accountancy Arusha, University of Dar es salaam and supervisors for their support.

Conflicts of Interest

The authors declare that there are no conflicts of interest to disclose.

REFERENCES

Ahmed B, Hayat T, Abbasi FM and Alsaedi A 2021 Mixed convection and thermal radiation effect on MHD peristaltic motion of Powell-Eyring nanofluid. *Int. Communicat. Heat nd Mass Transfer*. 126**:** 105320.

Alam MS, Khatun MA, Rahman MM and Vajravelu K 2016 Effects of variable fluid properties and thermophoresis on unsteady forced convective boundary layer flow along a permeable stretching/shrinking wedge with variable Prandtl and Schmidt numbers. *Int. J. Mech. Sci.* 105:191-205.

Ali MY, Uddin MN, Uddin MJ and Zahed NR 2015 Similarity solutions of unsteady convective boundary layer flow along isothermal vertical plate with porous medium. *Open J. Fluid Dynam.* **5**(4):391-406.

Das S, Jana RN and Makinde OD 2015 Magnetohydrodynamic mixed convective slip flow over an inclined porous plate with viscous dissipation and Joule heating. *Alexandria Eng. J.* 54(2):251-261

Ganapathirao M and Ravindran R 2015 Non-uniform slot suction/injection into mixed convective MHD flow over a vertical wedge with chemical reaction. *Procedia Eng.* 127: 1102-1109.

Hossain MA, Roy NC and Siddiqa S 2017 Unsteady mixed convection dusty fluid flow past a vertical wedge due to small fluctuation in free stream and surface temperature. *Appl. Math. Comput*. 293:480-492.

Hussain M, Ghaffar A, Ali A, Shahzad A, Nisar KS, Alharthi MR and Jamshed W 2021 MHD thermal boundary layer flow of a Casson fluid over a penetrable stretching wedge in the existence of nonlinear radiation and convective boundary condition. *Alexandria Engin. J.* 60(6): 5473-5483.

James M, Mureithi EW and Kuznetsov D 2015 Effects of variable viscosity of nanofluid flow over a permeable wedge embedded in saturated porous medium with chemical reaction and thermal radiation. *Int. J. Adv. Appl. Math. Mech.* **2**(3):101-118.

Kitengeso R, Mureithi E, James M and Mango J 2018 Effects of magnetic fields on an unsteady mixed convective boundary layer flow of an electrically conducting fluid with temperature dependent properties. *Tanz. J. Sci*. 44(3):103-114.

Khan MWA, Khan MI, Hayat T and Alsaedi A 2020 Numerical solution of MHD flow of power law fluid subject to convective boundary conditions and entropy generation. *Comput. Method Progr. Biomed*. 188:105262.

Kumari M and Nath G 2010 Unsteady MHD mixed convection flow over an impulsively stretched permeable vertical surface in a quiescent fluid. *Int. J. NonLin. Mech.* 45(3):310-319.

Megahed AM, Reddy MG and Abbas W 2021 Modeling of MHD fluid flow over an unsteady stretching sheet with thermal radiation, variable fluid properties and heat flux. *Math. Comput. Simulat*. 185:583-593.

Mureithi E 2014 A mixed convection boundary layer flow over a vertical wall in a porous medium, with exponentially varying fluid viscosity. *J. Appl. Math. Phys.* 2014.

Nadeem S, Haq RU and Khan ZH 2014 Numerical study of MHD boundary layer flow of a Maxwell fluid past a stretching sheet in the presence of nanoparticles. J. *Taiwan Inst. Chem. Eng.* 45(1):121-126.

Nazar R, Amin N and Pop I 2004 Unsteady mixed convection boundary layer flow near the stagnation point on a vertical surface in a porous medium. *Int. J. Heat Mass Transfer*. 47(12-13):2681-2688.

Olanrewaju PO, Anake T, Arulogun OT, Ajadi DA 2012 Further results on the effects of variable viscosity and magnetic

field on flow and heat transfer to a continuous flat plate in the presence of heat generation and radiation with a Convective boundary condition. *Am. J. Comput. Appl. Math.* 2012, **2**(2):42-48.

Pavlov KB 1974 Magnetohydrodynamic flow of an incompressible viscous fluid caused bydeformation of a plane surface. *Magnit. Gidrodinam.* 4(1)(146-147).

Raje A, Bhise AA and Kulkarni A 2023 Entropy analysis of the MHD Jeffrey fluid flow in an inclined porous pipe with convective boundaries. *Int. J. Thermofluids*, 17:100275.

Rana P, Bhargava R and Beg OA 2012 Numerical solution for mixed convection bound-´ ary layer flow of a nanofluid along an inclined plate embedded in a porous medium. *Comput. Math. Applicat.*. **64**(9):2816-2832.

Reddy BP 2016 Mass transfer effects on an unsteady MHD free convective flow of an incompressible viscous dissipative fluid past an infinite vertical porous plate. *Int. J. Appl. Mech. Eng.*. **21**(1):143-155.

Reddy SRR and Reddy PBA 2022 Thermal radiation effect on unsteady three-dimensional MHD flow of micropolar fluid over a horizontal surface of a parabola of revolution. *Propulsion and Power Research*. **11**(1):129-142.

Saqib M, Hanif H, Abdeljawad T, Khan I, Shafie S and Nisar KS 2020 Heat transfer in mhd flow of maxwell fluid via fractional cattaneo-friedrich model: A finite difference approach. *Comput. Mater. Contin.* **65(**3):1959-1973.

Sattar MA 2013 Derivation of the similarity equation of the 2-D unsteady boundary layer equations and the corresponding similarity conditions. *Am. J. Fluid Dynam.* **3**(5):135.

Sivasankaran S, Bhuvaneswari M and Alzahrani AK 2020 Numerical simulation on convection of non-Newtonian fluid in a porous enclosure with non-uniform heating and thermal radiation. *Alexandria Eng. J.* **59(**5):3315-3323.

Schlichting H 1979 Boundary-Layer Theory, 7th edn McGraw-Hill.

Vajravelu K, Prasad KV and Ng CO 2013 Unsteady convective boundary layer flow of a viscous fluid at a vertical surface with variable fluid properties. *Nonlin. Anal: Real World Applicat.*. ***14(1):455-464.***

Zainal NA, Nazar R, Naganthran K and Pop I 2021 Heat generation/absorption effect on MHD flow of hybrid nanofluid over bidirectional exponential stretching/shrinking sheet. *Chin. J. Phys.* **69**:118-133.